

---

# On the Importance of Multistability for Horizon Generalization in Reinforcement Learning

---

**Asad Bakija**

Dept. of Electrical Engineering and Computer Science  
University of Liège  
Liège, Belgium  
Asad.Bakija@uliege.be

**Florent De Geeter**

University of Liège

**Julien Brandoit**

University of Liège

**Pierre Sacré**

University of Liège

**Guillaume Drion**

University of Liège  
gdrion@uliege.be

## Abstract

In reinforcement learning (RL), agents acting in partially observable Markov decision processes (POMDPs) must rely on memory, typically encoded in a recurrent neural network (RNN), to integrate information from past observations. Long-horizon POMDPs, in which the relevant observation and the optimal action are separated by many time steps (called the horizon), are particularly challenging: training suffers from poor generalization, severe sample inefficiency, and prohibitive exploration costs. Ideally, an agent trained on short horizons would retain optimal behavior at arbitrarily longer ones, but no formal framework currently characterizes when this is achievable. To fill this gap, we formalized *temporal horizon generalization*, the property that a policy remains optimal for all horizons, derived a necessary and sufficient condition for it, and experimentally evaluated the ability of nonlinear and parallelizable RNN variants to achieve it. This paper presents the resulting theoretical framework, the empirical evaluation, and the dynamical interpretation linking RNN behavior to temporal horizon generalization. Our analyses reveal that multistability is necessary for temporal horizon generalization and, in simple tasks, sufficient; more complex tasks further require transient dynamics. In contrast, modern parallelizable architectures, namely state space models and gated linear RNNs, are monostable by construction and consequently fail to generalize across temporal horizons. We conclude that multistability and transient dynamics are two essential and complementary dynamical regimes for horizon generalization, and that no current parallelizable RNN exhibits both. Designing parallelizable architectures that combine these regimes thus emerges as a key direction for scalable long-horizon RL.

## 1 Introduction

Reinforcement learning (RL) typically requires collecting large amounts of data through interactions with the environments, making the learning process slow and time-consuming. Sparse-reward environments, in which rewards are only given when reaching a limited subset of states, aggravate the problem by making exploration even more complicated. Rather than directly training on difficult

environments, generalization provides an alternative by allowing an agent trained on a simpler version to handle more complex variations. Not only does this approach allow to tackle tasks for which direct learning is untractable, but it also drastically reduces exploration cost and training duration.

However, generalization remains a fundamental challenge, as learned policies can easily struggle to generalize across variations of the training environment. A fundamental driver of overfitting is incomplete exploration of high-dimensional Markov decision processes (MDPs) [1]. This leads to non-robust policies, whose decisions can become unpredictable when facing unusual situations, even if the environment is fully-observable [2]. This issue is further exacerbated in partially observable Markov decision processes (POMDPs) due to the inherent epistemic uncertainty.

Myers et al. [3] introduced a property called *horizon generalization*, defined as the ability to learn from short-horizon tasks and generalize to long-horizon tasks. They connected this property to planning invariance, where agents take the same decisions regardless of whether they are given a distant goal or an intermediate waypoint. In this work, we extend this idea to long-horizon POMDPs, in which the relevant observation and the optimal action are separated by many time steps called the horizon  $T$ , but the optimal action is independent of this horizon. In this context, we introduce a property called *temporal horizon generalization* (THG), the ability of a policy trained on an horizon  $T$  to remain optimal for all horizons  $T \geq 0$ . We also connect this property with specific dynamical regimes of recurrent neural networks (RNNs), that are the typical architecture used to tackle POMDPs (a more detailed related work is provided in Section A). Our main contributions are as follows.

**Definition and condition for THG.** We provide a general definition of THG, as well as a necessary and sufficient condition to achieve it in arbitrary partially observable RL settings. We further show that multistability, the coexistence of multiple stable equilibria in intrinsic memory dynamics, is critical to achieve THG.

**Monostability and multistability in classical and parallelizable RNNs.** We connect this multistability property with the dynamics of RNNs, showing that classical nonlinear RNNs can reach multistability but not state-of-the-art parallelizable RNNs such as state-space models (SSMs) [4–6] and linear gated RNNs [7–11].

**THG in POMDPs.** We validate our theoretical findings experimentally on two POMDP environments, showing that nonlinear RNNs exploit multistability to reach THG, and that SSMs and linear gated RNNs indeed lack THG capacity. We further show that THG-capable models trained on simple tasks are better at solving more complex tasks than models directly trained on the more complex one. We then isolate the role of multistability in THG by using the bistable memory recurrent units (BMRU) [12], a recently proposed parallelizable model, that is bistable while lacking transient dynamics.

**Transient dynamics vs multistability in THG.** Finally, we highlight the essential synergy between transient dynamics and multistability, particularly in environments defined by a mix of sparse, critical cues and frequently updated observations.

As parallelizable RNN architectures, specifically SSMs and linear gated RNNs, are increasingly becoming the standard for scalability, our research highlights the limitations of uniform architectures in RL. *We advocate for the use of hybrid parallelizable frameworks that effectively leverage the benefits of transient dynamics alongside multistability.*

## 2 Multistability and temporal horizon generalization

Proofs for all theorems and propositions can be found in Section B.

### 2.1 Definition of temporal horizon generalization

We consider a sparse, partially observable reinforcement learning problem. An agent acts in an environment with observation space  $\mathcal{O}$  and action space  $\mathcal{A}$ . At each time step  $t$ , the agent updates an internal (hidden) state  $h_t \in \mathcal{H}$  according to

$$h_t = f(h_{t-1}, o_t, a_{t-1}), \tag{1}$$

where  $o_t \in \mathcal{O}$  is the current observation and  $a_{t-1} \in \mathcal{A}$  is the previous action. The agent then selects  $a_t = \pi(h_t)$ , where  $\pi$  is the policy.

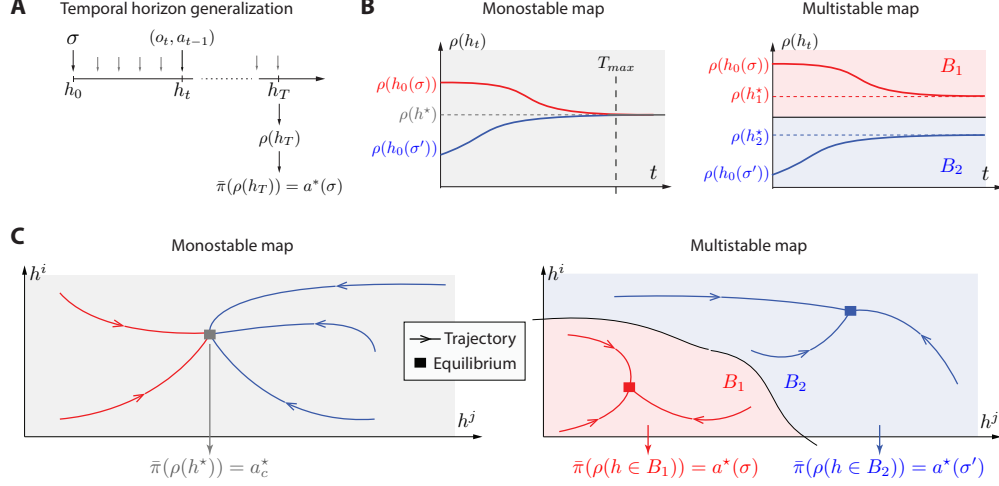


Figure 1: **Temporal horizon generalization.** **A.** Schematic definition of temporal horizon generalization. **B.** Sketch of time evolutions for a monostable map (left) and a multistable map (right). The red and blue color depicts the basin of attractions of each fixed point in the multistable case. **C.** Sketch of trajectories for a monostable map (left) and a multistable map (right) in the phase plane. The red and blue color depicts the basin of attractions of each fixed point in the multistable case.

Suppose the environment presents a key observation  $\sigma \in \mathcal{O}$  at time  $t = 0$ , which is encoded in the state  $h_0(\sigma)$ . It then provides observations  $o_t \in \mathcal{O}$  uninformative about  $\sigma$  paired with actions  $a_t \in \mathcal{A}$  during the next  $T - 1$  steps, called the idle phase. At step  $T$ , called the horizon, the agent must take the optimal action  $a^*(\sigma) \in \mathcal{A}$ , which depends on the value of  $\sigma$ .

**Definition 2.1** (Temporal horizon generalization). An agent is said to *generalize over temporal horizon* if the policy is optimal for all horizons  $T \geq 0$ . That is, a same policy solves the task regardless of the length of the idle phase (Figure 1A).

## 2.2 The simpler case of constant idle dynamics

**Simplified dynamics during the idle phase.** We first define a simplified idle phase ( $t = 1, \dots, T$ ) with constant observation  $o_t = o_c$  and constant actions  $a_{t-1} = a_c$ . The update reduces to a fixed map on  $\mathcal{H}$ :

$$U(h) := f(h, o_c, a_c). \quad (2)$$

We write  $U^T$  for the  $T$ -fold composition of  $U$  with itself. At the decision step  $T$ , the internal state is  $h_T = U^T(h_0(\sigma))$ .

**Condition for temporal horizon generalization** We introduce a *read-out function*  $\rho : \mathcal{H} \rightarrow \mathcal{D}$ , where  $\mathcal{D}$  is the space of decision-relevant representations. This read-out function extracts the relevant information to solve the task from  $h_t$  at any time. The policy decomposes as  $\pi(h_t) = \bar{\pi}(\rho(h_t))$ .

**Definition 2.2** (Compatible read-out). A function  $\rho : \mathcal{H} \rightarrow \mathcal{D}$  is *compatible* with the dynamics  $U$  if it is an invariant of  $U$ , i.e.,

$$\rho \circ U = \rho, \quad (3)$$

or equivalently  $\rho(U(h)) = \rho(h)$  for all reachable  $h \in \mathcal{H}$ . It is *separating* for  $\sigma$  if, for every pair  $\sigma \neq \sigma'$ ,

$$\rho(h_0(\sigma)) \neq \rho(h_0(\sigma')).$$

**Theorem 2.3** (Necessary and sufficient condition for horizon generalization). *Assume a policy  $\pi = \bar{\pi} \circ \rho$  that is optimal. The policy generalizes over temporal horizon,  $T \geq 1$ , if and only if  $\rho$  is a compatible and separating read-out in the sense of Definition 2.2.*

**Remark 2.4.** Condition (3) needs to hold only on states that are *reachable* after encoding some  $\sigma$ , i.e., on the set  $\{U^n(h_0(\sigma)) : \sigma \in \mathcal{O}, n \geq 0\}$ . It is not required for every  $h \in \mathcal{H}$ .

### 2.2.1 Monostability precludes temporal horizon generalization

**Definition 2.5** (Monostable map). The dynamics  $U : \mathcal{H} \rightarrow \mathcal{H}$  is *monostable* (or globally attracting) if it has a unique globally attracting fixed point  $h^* \in \mathcal{H}$ :

$$U^T(h) \longrightarrow h^* \quad \text{as } T \rightarrow \infty, \quad \forall h \in \mathcal{H}.$$

**Proposition 2.6** (Monostability precludes temporal horizon generalization). *Let  $U$  be monostable with attractor  $h^*$ . Let  $\rho : \mathcal{H} \rightarrow \mathcal{D}$  be any read-out function that is compatible with  $U$  in the sense of (3). Then  $\rho$  is constant on the basin of attraction of  $h^*$ , i.e.,  $\rho(h) = \rho(h^*)$  for all  $h \in \mathcal{H}$ . In particular,  $\rho$  cannot be separating for any two distinct observations  $\sigma \neq \sigma'$  (Figure 1B, left).*

**Corollary 2.7.** *In a monostable model, memory of past observations and temporal horizon generalization are fundamentally incompatible: no policy architecture can achieve both simultaneously.*

### 2.2.2 Multistability as a solution

**Definition 2.8** (Multistable map). The dynamics  $U : \mathcal{H} \rightarrow \mathcal{H}$  is *multistable* if it has at least two distinct attractors  $A_1, A_2 \subset \mathcal{H}$  with disjoint, non-empty basins of attraction  $B_1, B_2 \subset \mathcal{H}$ . Fixed-point attractors ( $A_i = \{h_i^*\}$ ) are the simplest case, but limit cycles or more general compact invariant sets are included.

**Theorem 2.9** (Multistability enables temporal horizon generalization). *Let  $U$  be multistable with attractors  $A_1, A_2$  and corresponding basins  $B_1, B_2$ . Suppose:*

- (i) *For each  $\sigma$ , the encoding places  $h_0(\sigma)$  in a specific basin  $B_{k(\sigma)}$ , i.e., the acquisition phase is well-posed.*
- (ii) *There exists a read-out  $\rho : \mathcal{H} \rightarrow \mathcal{D}$  that*
  - *is invariant within each basin:  $\rho(U(h)) = \rho(h)$  for all  $h \in B_k$ ,  $k = 1, 2$ , and*
  - *separates the basins:  $\rho(h) \neq \rho(h')$  with  $h \in B_1, h' \in B_2$ .*
- (iii) *The trajectory  $\{U^T(h_0(\sigma))\}_{T \geq 0}$  stays within  $B_{k(\sigma)}$  for all  $n$  (no crossing of basin boundaries).*

*Then the policy  $\pi = \bar{\pi} \circ \rho$  generalizes over all temporal horizons (Figure 1B, right).*

### 2.3 Extension to non-constant idle dynamics

In practice the agent keeps acting and observing even during the idle phase: observations fluctuate and the agent takes exploratory or habitual actions, or achieves intermediate goals. As long as these perturbations never push the hidden state across the boundary between two basins of attraction, the read-out  $\rho$  remains informative and temporal horizon generalization is preserved.

**Proposition 2.10** (Robustness to non-constant perturbations). *Let  $U_{o_t, a_{t-1}}(h) = f(h, o_t, a_{t-1})$  with potentially time-varying  $(o_t, a_{t-1})$ . Suppose:*

- (i) *There exist attracting regions  $B_1, B_2 \subset \mathcal{H}$  that are forward-invariant under every  $U_{o,a}$ :  $U_{o,a}(B_k) \subseteq B_k$  for all  $(o, a)$ .*
- (ii) *A read-out  $\rho$  is invariant within each  $B_k$  under every  $U_{o,a}$ :  $\rho(U_{o,a}(h)) = \rho(h)$  for all  $h \in B_k$ .*

*Then the conclusions of Theorem 2.9 hold with  $U^T$  replaced by the composition  $U_{o_T, a_{T-1}} \circ \dots \circ U_{o_1, a_0}$  (Figure 1C).*

## 3 Dynamics and multistability in RNNs

### 3.1 Nonlinear RNNs

RNNs encode time-dependencies in a recurrent hidden state  $h_t$  whose update depends on the previous hidden state  $h_{t-1}$  and current observation of a time-series  $x_t$ . It writes

$$h_t = f_\theta(h_{t-1}, x_t), \quad \forall t \geq 1, \quad (4)$$

where  $f_\theta$  represents the update equation of the RNN and  $\theta$  the learnable parameters of the network. Nonlinear versions such as LSTMs [13] and GRUs [14] have dominated sequence modeling for decades, but many variants such as Janet [15], (n)BRC [16], and MGU [17] have appeared over the years. Due to their recurrent nature, RNNs can encode time dependencies in their time-varying dynamics (Equation (4)), creating fading memory of past inputs.

Nonlinear RNNs can also exhibit multistability, the coexistence of multiple possible state values  $\bar{h}$  at equilibrium for a same constant input  $\bar{x}$ , making them compatible with Theorem 2.9. An RNN is multistable if its steady-state equation

$$\bar{h} - f_{\theta}(\bar{h}, \bar{x}) = 0, \quad (5)$$

admits multiple solutions for some set of constant input  $\bar{x}$ . Multistability allows for persistent memory under constant input value through a history-dependent convergence towards one of the multiple equilibria [16, 18]. Most nonlinear RNNs can reach multistability for some set of learnable parameters  $\theta$  [18]. In this work, we use the GRU, BRC and nBRC variants in our experiments (Section H).

### 3.2 Parallelizable RNNs

Recent efforts have led to the emergence of novel RNN architectures that are parallelizable over the sequence length with competitive performance on sequential benchmarks. In this section, we show that most state-of-the-art parallelizable RNN approaches lead to strictly monostable models, making them incompatible with Theorem 2.9, hence THG.

SSMs and linear RNNs exploit linear state dynamics to achieve parallelizable training, either through convolutional representations [4, 5] or the parallel scan algorithm [19, 7, 6]. The update equation of arbitrary linear RNNs writes  $h_t = A(x_t)h_{t-1} + B(x_t)x_t$ , where stability requires all eigenvalues of  $A(x_t)$  to be contained within the unit circle in the complex plane. The steady-state solutions  $\bar{h} = -(A(\bar{x}) - I)^{-1}B(\bar{x})\bar{x}$  are explicit, meaning that only one *and only one* solution  $\bar{h}$  exists for any input  $\bar{x}$ .

Gated RNNs can also achieve parallelizable training by removing the state dependency in their gating mechanisms, *i.e.*, computing gate values from the input alone,  $z_t = \sigma(W_z x_t)$ . Several such architectures have been proposed, including xLSTM [9], HGRN [8], MatMul-free LM [11], GILR [7], and minGRU [10], though some only achieve partial parallelization. It yields an update equation of the form  $h_t = (1 - z_t) \odot h_{t-1} + z_t \odot \tilde{h}_t$ , where  $\tilde{h}_t$  depends only on  $x_t$ . The steady-state solutions reduce to  $\bar{h} = \tilde{h} = \phi(W_h \bar{x})$  where  $\phi$  is an activation function whose structure is determined by the dynamical equation of  $\tilde{h}_t$ . The steady maps an explicit solution  $\bar{h}$  to any input value  $\bar{x}$ . This result extends to gated RNNs with multiple gates, provided that no gate is state-dependent. In this work, we use minGRU as a representative linear gated RNN (Section H).

### 3.3 Bistable memory recurrent unit

Memory recurrent units (MRUs) represent a class of parallelizable RNNs with properties complementary to those of linear RNNs: they exhibit multistability but lack transient dynamics (*i.e.*, they assume instantaneous convergence) [12]. At each timestep  $t$  and for a given input  $x_t$ , the MRU outputs a solution to the steady-state equation  $\tilde{h}_t - f_{\theta}(\tilde{h}_t, x_t) = 0$ . When multiple solutions exist, the previous state  $\tilde{h}_{t-1}$  determines the selected solution, effectively modeling history-dependent behavior. A prominent example is the bistable memory recurrent unit (BMRU), which integrates learnable hysteretic dynamics into a gated architecture [12]. In this work, we use the BMRU as a representative multistable model to contrast with the monostable nature of modern gated linear RNNs (Section H).

## 4 Experiments

For our experiments, we use the T-maze [20] and introduce an extension called the LookupTreeMaze (each environments are formally described in Section F and Section G, respectively).

In the T-maze (Figure 2A), the agent received an observation  $\sigma$  at the beginning of the maze that tells it the position of the reward at the end of the maze ( $\sigma = \text{up or down}$ ). The objective is to navigate the maze to reach the junction and make the correct decision  $a^*(\sigma)$  at the junction to receive the reward. The T-maze is a prototypical example to test THG, as the information and objective are separated by maze length (*i.e.*, defining the idle phase and the horizon). Although solving short T-maze environments is simple, solving long ones is known to be difficult.

The LookupTreeMaze extends this environment by connecting several T-mazes in series (Figure 2B). The agent receives a lookup table  $\sigma$  at the first time step that contains a random sampling of up

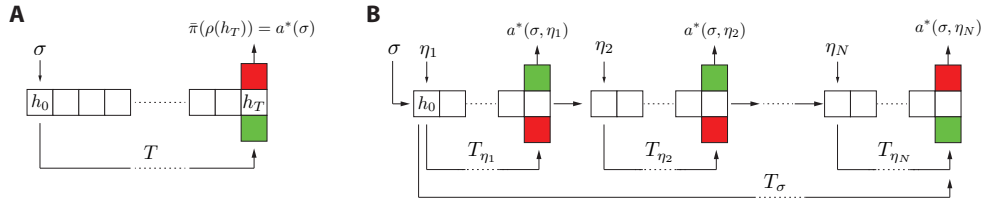


Figure 2: **Benchmarks.** **A.** Illustration of the T-maze environment. The starting observation  $\sigma$  serves as the instruction for the decision required at the end of the corridor, both separated by the horizon  $T$ . **B.** Illustration of the LookupTreeMaze environment. The starting observation  $\sigma$  provides an instruction table for the decision required at the end of each corridor, and the observations  $\eta_i$  tells where to read in the table  $\sigma$  to take the correct decision at the next junction. This environment has two intricate horizons:  $T_\sigma$ , which separates the observation  $\sigma$  provided at the start and each decisions, and  $T_{\eta_i}$ , which separates the observations  $\eta_i$  provided at the beginning of each T-maze and the decisions.

and down directions corresponding to positive reward directions, with at least one of each. At the beginning of each T-maze within the LookupTreeMaze, the agent receives an index  $\eta_i$  that references the position of the next reward in the lookup table. The objective is to navigate the maze to reach the next junction and make the correct decision  $a^*(\sigma, \eta_i)$  at each junction to receive the reward. This environment combines very sparse informative observations  $\sigma$  with frequently updated ones  $\eta_i$  and has two intricate horizons ( $T_\sigma$  and  $T_{\eta_i}$ ), allowing to test THG in the case of non-constant idle dynamics.

For each environment, we use two complementary approaches to test the connection between THG and RNN dynamics. In the first approach, we train nonlinear RNNs in a classical way, and compare performance and generalization capabilities with multistability a posteriori, allowing for unbiased evaluation. We then reproduce the experiments using minGRU as an example of parallelizable monostable RNN with transient dynamics and BMRU as an example of parallelizable bistable RNN without transient dynamics, allowing us to assess the role of each on THG separately.

We quantify model performance by computing the average sum of the rewards obtained during an episode. Multistability is quantified using the variability among attractors (VAA) metric [18] (see Section D): higher VAA values  $\in [0, 1]$  correspond to higher levels of multistability.

## 4.1 THG on the T-maze

### 4.1.1 THG in nonlinear RNNs

We first trained 90 models (30 GRU, 30 BRC and 30 nBRC) on two different T-maze environments (see Section E). The first one is a short-horizon problem: the T-maze length is randomly chosen between 1 and 3 for each new episode. The second one is a long-horizon problem: the T-maze length is fixed at 100. The models trained on shorter T-mazes learn an optimal policy in only a couple of training steps, with almost no variance. Those trained on longer T-mazes struggle to learn to solve the task properly and show high variance (the evolution of the rewards obtained by the agents during their training is provided in Section I). This result is expected in an RL setting, as exploration is much more difficult in long T-mazes, leading to unstable training.

We next tested whether training on T-mazes of length 100 improves model performance compared to first training on smaller T-mazes and evaluating on longer ones. To do so, we evaluated the models trained on both T-maze sizes on the T-maze of length 100. Figure 3A (top) shows the number of models that either never reach the end of the maze, choose a direction at random, or correctly solve the task for both the models trained on small T-mazes (blue) and the ones trained on the longer version (orange). The proportion of models that solve the task is almost equivalent for the two categories, showing that training on the large T-maze size provides little advantage as compared to training on smaller T-maze sizes, and it even leads to difficulties related to exploration. In addition, most models trained on smaller T-maze sizes reach the end of the longer T-maze, with half making the correct decision and the other half behaving at random. It suggests that these two subpopulations

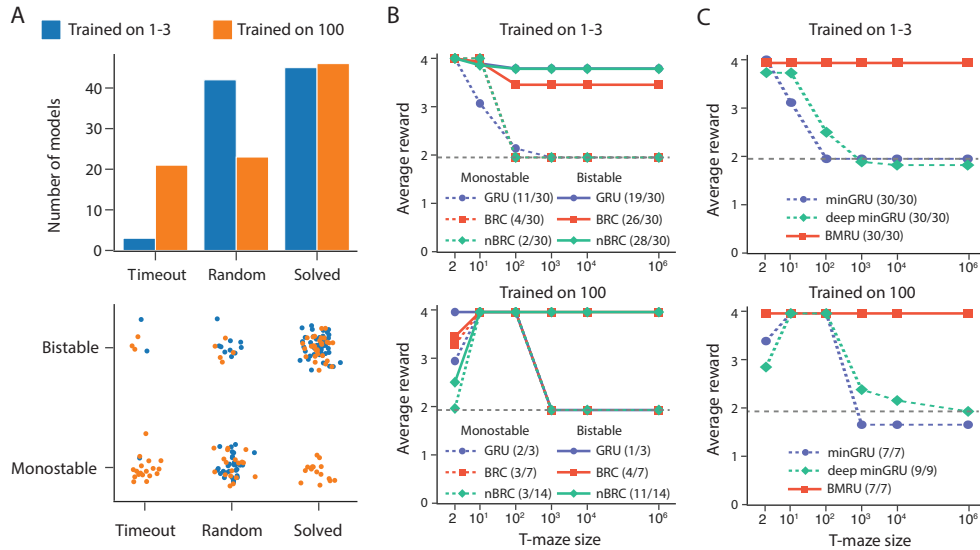


Figure 3: **Generalization capabilities on the T-maze.** **A.** Top, number of models that time-outed, reached the end but acted randomly, or solved the T-maze of size 100. Bottom, scatter plot of models separated by their performance (timeout, random or solved) and their monostable/bistable properties. Blue bars/scatters represent models trained on T-mazes of size 1-3, whereas orange bars/scatters represent models trained on T-mazes of size 100. **B.** Average reward obtained for each nonlinear RNN as a function of T-maze size. Models are separated into monostable models (dashed lines) and bistable models (full lines). **C.** Average reward obtained for each parallelizable RNN as a function of T-maze size. Models are separated into monostable models (dashed lines) and bistable models (full lines). The gray dashed line represents random guess.

solved the task on the shorter T-maze using two different memorization mechanisms, one leading to generalization, the other not.

#### 4.1.2 The role of multistability in THG

We assessed if these memorization mechanisms were linked to RNN monostable/multistable properties. Figure 3A (bottom) categorizes each model based on its performance on the long T-maze (timeout, random or solved) and its multistability properties (monostable or bistable). Each blue (resp. orange) dot corresponds to a model trained on the short (resp. long) T-maze. For the models trained on small T-mazes, the correlation between multistability and the ability to solve the environment (and therefore their generalization capability) is clear. No monostable model trained on the short T-maze solves the long one, whereas most bistable models do. This suggests that bistability (and more generally multistability) is a necessary condition for THG. The models directly trained on the longer T-mazes solve the environment using either slow transient dynamics or multistability. In addition, fewer models reached bistability in this case (57/90 for the short T-maze vs 36/90 for the long one). This suggests that training on long versions of the T-maze does not promote information encoding through multistability.

We then further evaluated THG capabilities of the models trained on either the short or the long T-maze on environments by testing them on T-mazes of length ranging from 2 to  $10^6$  (Figure 3B). Models are classified based on whether they were trained on small (top graph) or long (bottom graph) T-mazes, and their stability properties. Figure 3B, top confirms that bistability leads to generalization for arbitrary long T-mazes, and that this property is independent on model type: the same observation can be made for GRU, BRC and nBRC. The average rewards of monostable models converge to random, indicating that these models always forget the initial information and choose a random direction.

Figure 3B, bottom tells a more subtle story. Again, we observe that monostable models fail to generalize on longer mazes, whereas multistable models maintain their ability to generalize on longer

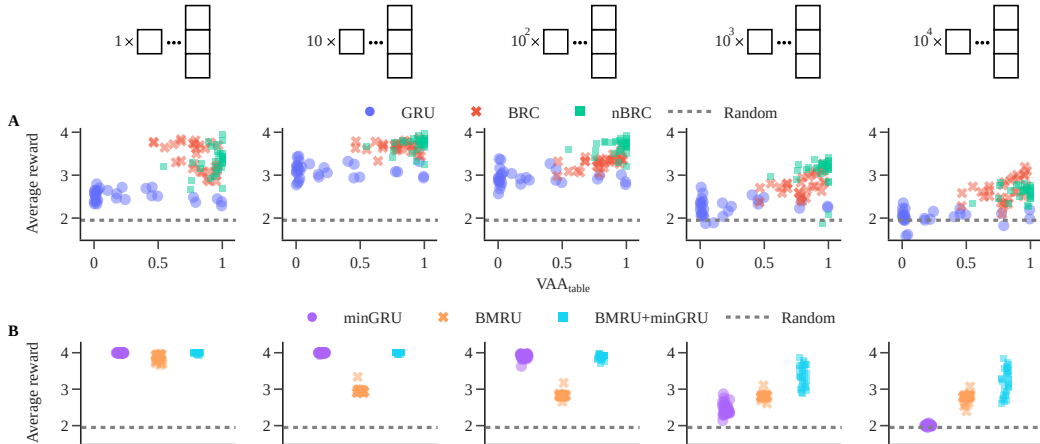


Figure 4: **Generalization capabilities on the LookupTreeMaze.** **A.** Average reward obtained by the nonlinear RNNs as a function of their VAA on different versions of the LookupTreeMaze. The number of mazes in the environment increases from left to right and is given at the top of the graph. A few points are out of scope (rewards axis) due to models timing out. **B.** Average reward obtained by the parallelizable RNNs as a function of their VAA on different versions of the LookupTreeMaze. The number of mazes in the environment increases from left to right and is given at the top of the graph. A few points are out of scope (rewards axis) due to models timing out.

mazes, but not on shorter T-mazes. This is due to the fact that even multistable models require transient dynamics to reach equilibrium, which are considerably slower when trained on longer mazes (Section I). These transient dynamics might lead to erroneous decisions, as they were not exploited during training. These results suggest that training a multistable model on shorter rather than longer T-mazes not only helps training capabilities and efficiency, but also leads to improved THG.

#### 4.1.3 THG in parallelizable RNNs

We then reproduced the same experiments using the parallelizable RNN variants minGRU and BMRU (Figure 3C). The results show a similar trend than those of nonlinear RNNs: fewer models solve the task when trained on long-horizon (23/90) than on short horizon (90/90), and monostable minGRU fails to generalize on either shorter or longer mazes, whereas multistable BMRU generalizes to all maze sizes in all conditions. The fact that BMRU generalizes also on shorter mazes comes from the absence of transient dynamics by design: it converges to equilibrium in a single timestep, which further confirms our analysis above on the role of transient dynamics.

Monostable models such as minGRU can however create long-lasting fading memory if more neurons and more layers are used in the network, which could lead to improved generalization. We tested this possibility by training a deep minGRU variant (4 layers of 128 neurons instead of 1 layer of 5 neurons). Although increasing network size indeed slightly improves generalization capabilities, it remains significantly below the capabilities of the small multistable network, which achieves true THG.

## 4.2 THG on the LookupTreeMaze

The added difficulty in the LookupTreeMaze to THG is twofold: the models have to retain more information, but also be able to use the information stored in their state several times. We train all models on a random number of T-mazes, between 1 and 20, with maze sizes chosen uniformly from 1 to 3, and all models manage to learn the task (Section I). We next evaluate the generalization capabilities of each models on longer versions of the environment by increasing the number of T-mazes.

#### 4.2.1 Nonlinear RNNs on the LookupTreeMaze

We first investigate the ability of nonlinear RNNs to generalize on the number of T-mazes by evaluating all 90 models on several LookupTreeMazes with increasing number of mazes (length of 3). To observe the impact of multistability on the generalization, the VAA, as described in Section D, is computed to measure how well the lookup table is encoded in stable states. The information to encode in this task is no longer a single bit, therefore there is not anymore a clear distinction between monostable or multistable models. In the following observation, we call *monostable* models the ones with a VAA close to 0, as opposed to the *multistable* ones, whose VAA are close to 1.

All nonlinear models perform reasonably well with 10 T-mazes, which is the mean number they saw during training (Figure 4A). Model performance tends to decrease when the number of T-mazes increase, but the degradation is more present for models with a low VAA, which highlights the important role played by multistability. Degradation is however also present in highly multistable models, showing that multistability alone is not sufficient in more complex environments, but a mix of multistability and transient dynamics might be required. However, it is difficult to assess the role of each dynamical regimes on nonlinear RNNs, as both are intimately linked.

#### 4.2.2 The synergy between transient dynamics and multistability in THG

We therefore reproduced the same experiments using the parallelizable RNN variants minGRU (purple dots in Figure 4) and BMRU (orange crosses in Figure 4), in order to isolate the role of transient dynamics and multistability on solving the task. The results showed an interesting trend: minGRU is much more efficient than BMRU at solving the tasks for up to 100 T-mazes, but does not generalize to arbitrary horizons (the performance becomes random for all models at 10 000 mazes). BMRU is however less efficient, but maintains a stable, above average performance even for a large number of T-mazes, showing that at least a subset of models achieve THG. This shows that, for environments that combine sparse observations with frequently updated ones, transient dynamics and multistability are both essential.

To test the combined roles of both dynamical regimes, we reproduced the experiment with an hybrid architecture that is composed of half minGRU and half BMRU (blue squares in Figure 4). This hybrid architecture combines the capabilities of both minGRU and BMRU: THG with high performance on a small number of T-mazes. It even largely outperforms both architectures for a high number of T-mazes, some models maintaining an almost optimal policy to up to 10 000 T-mazes. These results highlight an essential synergy between transient dynamics and multistability in solving long-horizon, potentially complex tasks. These experiments also outline a solution to make this synergy compatible with parallelizability, providing a path towards scalable, efficient models with THG capabilities.

## 5 Discussion

In this paper, we introduced the concept of temporal horizon generalization in RL, showed how it can reduce exploration cost and training duration, and linked the ability of RNN variants to reach THG with their dynamical properties. Through a mix of theoretical developments and experimental validations, we have shown that multistability is a critical property for THG, and that this property is absent in most state-of-the-art parallelizable RNN variants, advocating against the use of monolithic parallelizable architectures.

**Limitations.** We address the limitations of our current approach and propose several promising avenues for future research.

*On the sufficiency of multistability.* While our theoretical results establish multistability as a necessary and sufficient condition for the existence of optimal policies with THG capabilities, reaching these policies during training is not guaranteed. This discrepancy is evidenced by our T-maze experiments: agents trained on long horizons successfully generalized to even longer sequences, yet failed on shorter ones. Developing generalization-aware training strategies would be an essential step to fully exploit the ability of multistable models to generalize.

*The switch towards parallelizable architectures.* As the field trends toward parallelizable RNN variants to enable large-scale computation, a critical trade-off has emerged. We have demonstrated that current state-of-the-art models such as including SSMs [7, 4–6] and gated parallel RNN [7–11]

are inherently monostable, which fundamentally limits their THG capabilities. As a solution, we propose a shift toward hybrid architectures that integrate the efficiency of parallelizable transient dynamics with the robust memory of multistability. While our current experiments serve as a proof-of-concept, further research into these hybrid designs could lead to scalable, efficient models capable of true multistability-based horizon generalization.

*THG in more complex benchmarks.* We empirically validated our theoretical findings using two environments specifically designed to isolate the effects of THG. While this focused approach allowed for a rigorous assessment of model capabilities, extending this analysis to more complex benchmarks is an important future direction. Investigating the interplay between multistability and THG in environments with multiple, competing objectives and nested temporal horizons will further clarify their practical significance.

## Acknowledgements

This present research was supported by the Belgian Government through the Federal Public Service Policy and Support. It also benefited from computational resources made available on Lucia, the Tier-1 supercomputer of the Walloon Region, infrastructure funded by the Walloon Region under the grant agreement n°1910247. Florent De Geeter gratefully acknowledges the financial support of the Walloon Region for Grant No. 2010235 – ARIAC by DW4AI.

## References

- [1] Ezgi Korkmaz. A survey analyzing generalization in deep reinforcement learning. <https://arxiv.org/pdf/2401.02349v2>, 2024.
- [2] Dibya Ghosh, Jad Rahme, Aviral Kumar, Amy Zhang, Ryan P Adams, and Sergey Levine. Why generalization in rl is difficult: Epistemic pomdps and implicit partial observability. *Advances in neural information processing systems*, 34:25502–25515, 2021.
- [3] Vivek Myers, Catherine Ji, and Benjamin Eysenbach. Horizon generalization in reinforcement learning. In *The Thirteenth International Conference on Learning Representations*, 2025.
- [4] Albert Gu, Isys Johnson, Karan Goel, Khaled Saab, Tri Dao, Atri Rudra, and Christopher Ré. Combining recurrent, convolutional, and continuous-time models with linear state space layers. *Advances in neural information processing systems*, 34:572–585, 2021.
- [5] Albert Gu, Karan Goel, and Christopher Re. Efficiently modeling long sequences with structured state spaces. In *International Conference on Learning Representations*, 2022.
- [6] Albert Gu and Tri Dao. Mamba: Linear-Time Sequence Modeling with Selective State Spaces. In *First Conference on Language Modeling*, August 2024.
- [7] Eric Martin and Chris Cundy. Parallelizing linear recurrent neural nets over sequence length. In *International Conference on Learning Representations*, 2018.
- [8] Zhen Qin, Songlin Yang, and Yiran Zhong. Hierarchically Gated Recurrent Neural Network for Sequence Modeling. *Advances in Neural Information Processing Systems*, 36:33202–33221, December 2023.
- [9] Maximilian Beck, Korbinian Pöppel, Markus Spanring, Andreas Auer, Oleksandra Prudnikova, Michael Kopp, Günter Klambauer, Johannes Brandstetter, and Sepp Hochreiter. xLSTM: Extended Long Short-Term Memory. *Advances in Neural Information Processing Systems*, 37: 107547–107603, December 2024. doi: 10.52202/079017-3417.
- [10] Leo Feng, Frederick Tung, Hossein Hajimirsadeghi, Mohamed Osama, Yoshua Bengio, and Roland Memisevic. Were RNNs all we needed? *arXiv preprint arXiv:2410.01201*, 2024.
- [11] Rui-Jie Zhu, Yu Zhang, Steven Abreu, Ethan Sifferman, Tyler Sheaves, Yiqiao Wang, Dustin Richmond, Sumit Bam Shrestha, Peng Zhou, and Jason K. Eshraghian. Scalable MatMul-free language modeling, 2025. URL <https://arxiv.org/abs/2406.02528>.

- [12] Florent De Geeter, Gaspard Lambrechts, Damien Ernst, and Guillaume Drion. Parallelizable memory recurrent units. *arXiv preprint arXiv:2601.09495*, 2026.
- [13] Sepp Hochreiter and Jürgen Schmidhuber. Long short-term memory. *Neural Computation*, 9(8):1735–1780, 1997.
- [14] Kyunghyun Cho, Bart Van Merriënboer, Caglar Gulcehre, Dzmitry Bahdanau, Fethi Bougares, Holger Schwenk, and Yoshua Bengio. Learning phrase representations using RNN encoder-decoder for statistical machine translation. In *Proceedings of the 2014 Conference on Empirical Methods in Natural Language Processing (EMNLP)*, pages 1724–1734, 2014.
- [15] Jos Van Der Westhuizen and Joan Lasenby. The unreasonable effectiveness of the forget gate. *arXiv preprint arXiv:1804.04849*, 2018.
- [16] Nicolas Vecoven, Damien Ernst, and Guillaume Drion. A bio-inspired bistable recurrent cell allows for long-lasting memory. *PLoS ONE*, 16(6):e0252676, 2021.
- [17] Guo-Bing Zhou, Jianxin Wu, Chen-Lin Zhang, and Zhi-Hua Zhou. Minimal gated unit for recurrent neural networks. *International Journal of Automation and Computing*, 13(3):226–234, 2016.
- [18] Gaspard Lambrechts, Florent De Geeter, Nicolas Vecoven, Damien Ernst, and Guillaume Drion. Warming up recurrent neural networks to maximise reachable multistability greatly improves learning. *Neural Networks*, 166:645–669, 2023.
- [19] Guy E. Blelloch. Scans as primitive parallel operations. *IEEE Transactions on Computers*, 38(11):1526–1538, November 1989.
- [20] Bram Bakker. Reinforcement learning with long short-term memory. *Advances in neural information processing systems*, 14, 2001.
- [21] Amy Zhang, Nicolas Ballas, and Joelle Pineau. A dissection of overfitting and generalization in continuous reinforcement learning. *arXiv preprint arXiv:1806.07937*, 2018.
- [22] Karl Cobbe, Oleg Klimov, Chris Hesse, Taehoon Kim, and John Schulman. Quantifying generalization in reinforcement learning. In *International conference on machine learning*, pages 1282–1289. PMLR, 2019.
- [23] Karl Cobbe, Chris Hesse, Jacob Hilton, and John Schulman. Leveraging procedural generation to benchmark reinforcement learning. In *International conference on machine learning*, pages 2048–2056. PMLR, 2020.
- [24] Robert Kirk, Amy Zhang, Edward Grefenstette, and Tim Rocktäschel. A survey of zero-shot generalisation in deep reinforcement learning. *Journal of Artificial Intelligence Research*, 76: 201–264, 2023.
- [25] Yoshua Bengio, Jérôme Louradour, Ronan Collobert, and Jason Weston. Curriculum learning. In *Proceedings of the 26th annual international conference on machine learning*, pages 41–48, 2009.
- [26] Sanmit Narvekar, Bei Peng, Matteo Leonetti, Jivko Sinapov, Matthew E Taylor, and Peter Stone. Curriculum learning for reinforcement learning domains: A framework and survey. *Journal of Machine Learning Research*, 21(181):1–50, 2020.
- [27] Josh Tobin, Rachel Fong, Alex Ray, Jonas Schneider, Wojciech Zaremba, and Pieter Abbeel. Domain randomization for transferring deep neural networks from simulation to the real world. In *2017 IEEE/RSJ international conference on intelligent robots and systems (IROS)*, pages 23–30. IEEE, 2017.
- [28] Leslie Pack Kaelbling, Michael L Littman, and Anthony R Cassandra. Planning and acting in partially observable stochastic domains. *Artificial intelligence*, 101(1-2):99–134, 1998.
- [29] Matthew J Hausknecht and Peter Stone. Deep recurrent q-learning for partially observable mdps. In *AAAI fall symposia*, volume 45, page 141, 2015.

- [30] Volodymyr Mnih, Koray Kavukcuoglu, David Silver, Andrei A Rusu, Joel Veness, Marc G Bellemare, Alex Graves, Martin Riedmiller, Andreas K Fidjeland, Georg Ostrovski, et al. Human-level control through deep reinforcement learning. *nature*, 518(7540):529–533, 2015.
- [31] Volodymyr Mnih, Adria Puigdomenech Badia, Mehdi Mirza, Alex Graves, Timothy Lillicrap, Tim Harley, David Silver, and Koray Kavukcuoglu. Asynchronous methods for deep reinforcement learning. In *International conference on machine learning*, pages 1928–1937. PmLR, 2016.
- [32] John Schulman, Filip Wolski, Prafulla Dhariwal, Alec Radford, and Oleg Klimov. Proximal policy optimization algorithms. *arXiv preprint arXiv:1707.06347*, 2017.
- [33] Alex Graves, Greg Wayne, and Ivo Danihelka. Neural turing machines. *arXiv preprint arXiv:1410.5401*, 2014.
- [34] Alex Graves, Greg Wayne, Malcolm Reynolds, Tim Harley, Ivo Danihelka, Agnieszka Grabska-Barwińska, Sergio Gómez Colmenarejo, Edward Grefenstette, Tiago Ramalho, John Agapiou, et al. Hybrid computing using a neural network with dynamic external memory. *Nature*, 538(7626):471–476, 2016.
- [35] Emilio Parisotto, Francis Song, Jack Rae, Razvan Pascanu, Caglar Gulcehre, Siddhant Jayakumar, Max Jaderberg, Raphael Lopez Kaufman, Aidan Clark, Seb Noury, et al. Stabilizing transformers for reinforcement learning. In *International conference on machine learning*, pages 7487–7498. PMLR, 2020.
- [36] Danijar Hafner, Timothy Lillicrap, Jimmy Ba, and Mohammad Norouzi. Dream to Control: Learning Behaviors by Latent Imagination. In *International Conference on Learning Representations*, September 2019.
- [37] Danijar Hafner, Timothy P Lillicrap, Mohammad Norouzi, and Jimmy Ba. Mastering atari with discrete world models. In *International Conference on Learning Representations*, 2020.
- [38] Danijar Hafner, Jurgis Pasukonis, Jimmy Ba, and Timothy Lillicrap. Mastering diverse control tasks through world models. *Nature*, 640(8059):647–653, 2025.
- [39] Luisa Zintgraf, Sebastian Schulze, Cong Lu, Leo Feng, Maximilian Igl, Kyriacos Shiarlis, Yarin Gal, Katja Hofmann, and Shimon Whiteson. Varibad: Variational bayes-adaptive deep rl via meta-learning. *Journal of Machine Learning Research*, 22(289):1–39, 2021.
- [40] Stephen Boyd and Leon O. Chua. Fading memory and the problem of approximating nonlinear operators with Volterra series. *IEEE Transactions on Circuits and Systems*, 32(11):1150–1161, 1985.
- [41] Razvan Pascanu, Tomas Mikolov, and Yoshua Bengio. On the difficulty of training recurrent neural networks. In *International conference on machine learning*, pages 1310–1318. PMLR, 2013.
- [42] Gustave Bainier, Antoine Chaillet, Rodolphe Sepulchre, and Alessio Frangi. State-space fading memory. *arXiv preprint arXiv:2603.23814*, 2026.
- [43] Peng Liu, Jun Wang, and Zhigang Zeng. An overview of the stability analysis of recurrent neural networks with multiple equilibria. *IEEE Transactions on Neural Networks and Learning Systems*, 34(3):1098–1111, 2023. doi: 10.1109/TNNLS.2021.3105519. Epub 2023 Feb 28.
- [44] Volodymyr Mnih, Adria Puigdomenech Badia, Mehdi Mirza, Alex Graves, Timothy Lillicrap, Tim Harley, David Silver, and Koray Kavukcuoglu. Asynchronous methods for deep reinforcement learning. In *International conference on machine learning*, pages 1928–1937. PmLR, 2016.
- [45] Shengyi Huang, Rousslan Fernand Julien Dossa, Chang Ye, Jeff Braga, Dipam Chakraborty, Kinal Mehta, and JoÃGo GM AraÃsjo. Cleanrl: High-quality single-file implementations of deep reinforcement learning algorithms. *Journal of Machine Learning Research*, 23(274):1–18, 2022.

## A Related Work

Since our work sits at the intersection of several active research areas, we briefly survey three relevant topics in this section: generalization in RL, memory for POMDPs, and multistability in RNNs.

**Generalization in reinforcement learning.** Generalization is a long-standing challenge in reinforcement learning: policies learned in one setting often fail to transfer even to superficially similar environments [1]. Early work highlighted that deep RL agents can overfit dramatically to the specifics of their training environments, including random seeds and initial state distributions, even when the underlying task remains the same [21]. This prompted the development of dedicated generalization benchmarks such as CoinRun [22] and Procgen [23], which expose policies to procedurally generated environments at test time, and systematic evaluations of what dimensions of variation agents can and cannot handle.

A comprehensive survey [24] categorizes generalization along several axes: across environment parameters (reward, dynamics, layout), across tasks, and across levels of difficulty, each presenting distinct failure modes. One practical strategy to improve generalization is curriculum learning, in which the agent is progressively exposed to harder instances of the task, reducing the exploration burden and improving sample efficiency [25, 26]. A closely related strategy is domain randomization, which widens the training distribution to encourage policies that are robust to unseen variations [27].

Generalization in fully observable settings is already difficult [2] and partial observability amplifies the difficulty because the agent cannot distinguish states that appear identical but require different actions.

Our work focuses on a specific, formally defined axis of generalization: the temporal horizon. Myers et al. [3] introduced *horizon generalization* in goal-conditioned MDPs and connected it to planning invariance, whereby an agent pursues the same policy regardless of whether it is given a distant goal or an intermediate waypoint. We extend this notion to the partially observable setting, where memory is the central bottleneck, and provide a formal necessary and sufficient condition that links horizon generalization to the dynamical properties of the agent recurrent memory. Crucially, unlike curriculum-based or domain-randomization approaches, which seek to generalize by widening the training distribution, temporal horizon generalization allows an agent trained exclusively on short horizons to remain optimal at arbitrarily longer ones, with no requirement to expose it to long-horizon episodes during training.

**Memory and recurrent architectures for POMDPs.** Partial observability is ubiquitous in real-world sequential decision making. A principled solution is to maintain a belief state, a probability distribution over the true environment state conditioned on the observation history [28]. Exact belief-state computation is generally intractable, and in deep RL it is typically replaced by a learned approximate summary encoded in the hidden state of a recurrent neural network. Hausknecht and Stone [29] proposed the deep recurrent Q-network (DRQN), which replaces one of the feedforward components of DQN [30] with an LSTM layer, showing that a recurrent hidden state can substitute for full observability in Atari games. Equipping actor-critic algorithms such as A3C [31] and PPO [32] with recurrent encoders has since become one of the standard approaches to handling partial observability.

Beyond standard RNNs, various approaches have been proposed to enhance the memory capacity accessible to the agent. Memory-augmented networks such as the neural Turing machine [33] and the differentiable neural computer [34] decouple capacity from the hidden-state dimension by equipping networks with an addressable external memory, enabling longer retention at the cost of additional architectural complexity. Transformer-based architectures provide a complementary strategy via self-attention over a growing context window. The gated transformer-XL (GTrXL) [35] adapts this idea for RL by incorporating gating to stabilize training, achieving strong results on memory-intensive benchmarks. However, self-attention is quadratic in context length, which becomes prohibitive for very long horizons, and attention over a finite window cannot provide the unbounded, perfectly persistent memory required for temporal horizon generalization.

Structured world models offer a further alternative, learning a latent dynamics model of the environment from which a compact belief state can be inferred. Dreamer and its successors [36–38] use a recurrent state space model to separate deterministic from stochastic latent dynamics, enabling

policy learning and value estimation through imagined rollouts. VariBAD [39] takes a Bayesian perspective, meta-learning a posterior over task parameters that is updated online to approximate the belief state. These approaches enrich memory through architectural or training innovations, but do not address the dynamical question of whether the underlying recurrent cell can sustain the persistent, history-dependent representations that temporal horizon generalization demands. Our analysis shows that this is fundamentally a question of multistability in the cell dynamics, a property that is absent in linear and input-gated architectures regardless of how they are embedded in a larger system.

**Multistability in RNNs.** Monostability and fading memory are closely related concepts [40]: a system with a single stable equilibrium forces all trajectories to decay exponentially toward that unique attractor, inevitably erasing information about past inputs, which is the key characteristic of fading memory [40–42]. In contrast, persistent memory requires multistability, where multiple distinct stable states can coexist, enabling the network to maintain and switch between stored values without asymptotic decay. Despite this fundamental link, *multistability remains largely neglected in the machine learning literature on recurrent architectures* [43]; notable exceptions include bio-inspired bistable cells [16, 18] and the MRU line of works [12], both of which explicitly harness multistable dynamics to overcome the inherent forgetting of monostable linear systems.

## B Temporal Horizon Generalization

### B.1 Definition of temporal horizon generalization

We consider a sparse, partially observable reinforcement learning problem. An agent acts in an environment with observation space  $\mathcal{O}$  and action space  $\mathcal{A}$ . At each time step  $t$ , the agent updates an internal (hidden) state  $h_t \in \mathcal{H}$  according to

$$h_t = f(h_{t-1}, o_t, a_{t-1}), \quad (6)$$

where  $o_t \in \mathcal{O}$  is the current observation and  $a_{t-1} \in \mathcal{A}$  is the previous action. The agent then selects  $a_t = \pi(h_t)$ , where  $\pi$  is the policy.

Suppose the environment presents a key observation  $\sigma \in \mathcal{O}$  at time  $t = 0$ , which is encoded in the state  $h_0(\sigma)$ . It then provides observations  $o_t \in \mathcal{O}$  uninformative about  $\sigma$  paired with actions  $a_t \in \mathcal{A}$  during the next  $T$  steps, called the idle phase. At step  $T$ , called the horizon, the agent must take the optimal action  $a^*(\sigma) \in \mathcal{A}$ , which depends on the value of  $\sigma$ .

**Definition B.1** (Temporal horizon generalization). An agent is said to *generalize over temporal horizon* if the policy is optimal for all horizons  $T \geq 0$ . That is, a same policy solves the task regardless of the length of the idle phase (Figure 1A).

### B.2 The simpler case of constant idle dynamics

**Simplified dynamics during the idle phase.** We first define a simplified idle phase ( $t = 1, \dots, T$ ) with constant observation  $o_t = o_c$  and constant actions  $a_{t-1} = a_c$ . The update reduces to a fixed map on  $\mathcal{H}$ :

$$U(h) := f(h, o_c, a_c). \quad (7)$$

We write  $U^T$  for the  $T$ -fold composition of  $U$  with itself. At the decision step  $T$ , the internal state is  $h_T = U^T(h_0(\sigma))$ .

**Condition for temporal horizon generalization** We introduce a *read-out function*  $\rho : \mathcal{H} \rightarrow \mathcal{D}$ , where  $\mathcal{D}$  is the space of decision-relevant representations. This read-out function extracts the relevant information to solve the task from  $h_t$  at any time. The policy decomposes as  $\pi(h_t) = \bar{\pi}(\rho(h_t))$ .

**Definition B.2** (Compatible read-out). A function  $\rho : \mathcal{H} \rightarrow \mathcal{D}$  is *compatible* with the dynamics  $U$  if it is an invariant of  $U$ , i.e.,

$$\rho \circ U = \rho, \quad (8)$$

or equivalently  $\rho(U(h)) = \rho(h)$  for all reachable  $h \in \mathcal{H}$ . It is *separating* for  $\sigma$  if, for every pair  $\sigma \neq \sigma'$ ,

$$\rho(h_0(\sigma)) \neq \rho(h_0(\sigma')).$$

**Theorem B.3** (Necessary and sufficient condition for horizon generalization). *Assume a policy  $\pi = \bar{\pi} \circ \rho$  that is optimal. The policy generalizes over temporal horizon,  $T \geq 1$ , if and only if  $\rho$  is a compatible and separating read-out in the sense of Definition 2.2.*

*Proof.* ( $\Rightarrow$ ) **Necessity.** Suppose the policy acts optimally at temporal horizon  $T$ . Then for every  $\sigma$ ,

$$\bar{\pi}(\rho(U^{T+1}(h_0(\sigma)))) = \bar{\pi}(\rho(U^T(h_0(\sigma)))) = a^*(\sigma),$$

where  $a^*(\sigma)$  denotes the correct action for  $\sigma$ . Since  $U^{T+1}(h_0(\sigma)) = U(U^T(h_0(\sigma)))$ , and since  $\bar{\pi}$  must distinguish different  $\sigma$ , we need  $\rho(U(h)) = \rho(h)$  for all states  $h$  reachable at step  $T$ . By induction this extends to all  $T \geq 0$ , giving  $\rho \circ U = \rho$  on all reachable states. Separability follows from the optimality assumption itself: the policy must produce different actions for different  $\sigma$ .

( $\Leftarrow$ ) **Sufficiency.** If  $\rho \circ U = \rho$ , then by induction  $\rho(U^T(h)) = \rho(h)$  for all  $T \geq 1$ . Therefore

$$\rho(U^{T+1}(h_0(\sigma))) = \rho(U^T(h_0(\sigma))) \quad \forall T \geq 1.$$

Since  $\rho$  is also separating, the policy  $\bar{\pi} \circ \rho$  recovers the correct action at every horizon.  $\square$

*Remark B.4.* Condition (3) needs to hold only on states that are *reachable* after encoding some  $\sigma$ , i.e., on the set  $\{U^n(h_0(\sigma)) : \sigma \in \mathcal{O}, n \geq 0\}$ . It is not required for every  $h \in \mathcal{H}$ .

### B.2.1 Monostability precludes temporal horizon generalization

**Definition B.5** (Monostable map).  $U : \mathcal{H} \rightarrow \mathcal{H}$  is *monostable* (or globally attracting) if it has a unique globally attracting fixed point  $h^* \in \mathcal{H}$ :

$$U^T(h) \longrightarrow h^* \quad \text{as } T \rightarrow \infty, \quad \forall h \in \mathcal{H}.$$

**Proposition B.6** (Monostability precludes temporal horizon generalization). *Let  $U$  be monostable with attractor  $h^*$ . Let  $\rho : \mathcal{H} \rightarrow \mathcal{D}$  be any read-out function that is compatible with  $U$  in the sense of (3). Then  $\rho$  is constant on the basin of attraction of  $h^*$ , i.e.,  $\rho(h) = \rho(h^*)$  for all  $h \in \mathcal{H}$ . In particular,  $\rho$  cannot be separating for any two distinct observations  $\sigma \neq \sigma'$  (Figure 1B, left).*

*Proof.* Let  $h \in \mathcal{H}$  be arbitrary. Since  $U$  is monostable,  $U^T(h) \rightarrow h^*$ . Using the invariance of  $\rho$  repeatedly:

$$\rho(h) = \rho(U(h)) = \rho(U^2(h)) = \dots = \rho(U^T(h)).$$

If  $\rho$  is continuous (a natural assumption for a learned read-out), then taking  $T \rightarrow \infty$  gives  $\rho(h) = \rho(h^*)$ .

Even without continuity, the invariance condition  $\rho \circ U = \rho$  implies that  $\rho$  is constant on every forward orbit  $\{U^T(h) : T \geq 0\}$ . Since all orbits converge to  $h^*$ , any two orbits eventually share the same state, so they must share the same value of  $\rho$ . Hence  $\rho$  cannot distinguish any two initial states, including  $h_0(\sigma)$  and  $h_0(\sigma')$  for  $\sigma \neq \sigma'$ .  $\square$

**Corollary B.7.** *In a monostable model, memory of past observations and temporal horizon generalization are fundamentally incompatible: no policy architecture can achieve both simultaneously.*

### B.2.2 Multistability as a solution

**Definition B.8** (Multistable map).  $U : \mathcal{H} \rightarrow \mathcal{H}$  is *multistable* if it has at least two distinct attractors  $A_1, A_2 \subset \mathcal{H}$  with disjoint, non-empty basins of attraction  $B_1, B_2 \subset \mathcal{H}$ . Fixed-point attractors ( $A_i = \{h_i^*\}$ ) are the simplest case, but limit cycles or more general compact invariant sets are included.

**Theorem B.9** (Multistability enables temporal horizon generalization). *Let  $U$  be multistable with attractors  $A_1, A_2$  and corresponding basins  $B_1, B_2$ . Suppose:*

- (i) *For each  $\sigma$ , the encoding places  $h_0(\sigma)$  in a specific basin  $B_{k(\sigma)}$ , i.e., the acquisition phase is well-posed.*
- (ii) *There exists a read-out  $\rho : \mathcal{H} \rightarrow \mathcal{D}$  that*
  - *is invariant within each basin:  $\rho(U(h)) = \rho(h)$  for all  $h \in B_k$ ,  $k = 1, 2$ , and*
  - *separates the basins:  $\rho(h) \neq \rho(h')$  with  $h \in B_1, h' \in B_2$ .*
- (iii) *The trajectory  $\{U^T(h_0(\sigma))\}_{T \geq 0}$  stays within  $B_{k(\sigma)}$  for all  $n$  (no crossing of basin boundaries).*

*Then the policy  $\pi = \bar{\pi} \circ \rho$  generalizes over all temporal horizons (Figure 1B, right).*

*Proof.* Fix  $\sigma$  and let  $k = k(\sigma)$ . By assumption (iii),  $U^T(h_0(\sigma)) \in B_k$  for all  $T \geq 0$ . By assumption (ii),  $\rho$  is invariant within  $B_k$ , so

$$\rho(U^{T+1}(h_0(\sigma))) = \rho(U^T(h_0(\sigma))) \quad \forall T \geq 0.$$

The policy therefore produces the same action at every horizon  $T$ . Since different  $\sigma$  values lead to different basins (assumption (i)), and  $\rho$  separates the basins (assumption (ii)), distinct  $\sigma$  values yield distinct read-outs, so the policy is correct for every  $\sigma$ .  $\square$

### B.3 Extension to non-constant idle dynamics

In practice the agent keeps acting and observing even during the idle phase: observations fluctuate and the agent takes exploratory or habitual actions, or achieves intermediate goals. As long as these perturbations never push the hidden state across the boundary between two basins of attraction, the read-out  $\rho$  remains informative and temporal horizon generalization is preserved.

**Proposition B.10** (Robustness to non-constant perturbations). *Let  $U_{o_t, a_{t-1}}(h) = f(h, o_t, a_{t-1})$  with potentially time-varying  $(o_t, a_{t-1})$ . Suppose:*

- (i) *There exist attracting regions  $B_1, B_2 \subset \mathcal{H}$  that are forward-invariant under every  $U_{o,a}$ :  $U_{o,a}(B_k) \subseteq B_k$  for all  $(o, a)$ .*
- (ii) *A read-out  $\rho$  is invariant within each  $B_k$  under every  $U_{o,a}$ :  $\rho(U_{o,a}(h)) = \rho(h)$  for all  $h \in B_k$ .*

*Then the conclusions of Theorem 2.9 hold with  $U^T$  replaced by the composition  $U_{o_T, a_{T-1}} \circ \dots \circ U_{o_1, a_0}$  (Figure 1C).*

*Proof.* By forward invariance,  $h_t \in B_{k(\sigma)}$  for all  $t \geq 0$ . By the invariance of  $\rho$  within  $B_k$ ,

$$\rho(h_T) = \rho(U_{o_T, a_{T-1}}(h_{T-1})) = \rho(h_{T-1}) = \dots = \rho(h_0).$$

The rest of the argument follows as in Theorem 2.9.  $\square$

## C Reinforcement Learning in POMDPs

Formally, a POMDP  $P$  is defined as an 8-tuple

$$P = (\mathcal{S}, \mathcal{A}, \mathcal{O}, p_0, T, R, O, \gamma),$$

where  $\mathcal{S}$  is the state space,  $\mathcal{A}$  is the action space, and  $\mathcal{O}$  is the observation space. The initial state distribution

$$p_0(s_0) : \mathcal{S} \rightarrow [0, 1]$$

gives the probability of  $s_0 \in \mathcal{S}$  being the initial state of the POMDP. The Markovian system dynamics are defined by the transition probability distribution

$$T(s_{t+1} | s_t, a_t) : \mathcal{S} \times \mathcal{A} \times \mathcal{S} \rightarrow [0, 1],$$

which gives the probability that taking action  $a_t \in \mathcal{A}$  in state  $s_t \in \mathcal{S}$  leads to state  $s_{t+1} \in \mathcal{S}$ . The reward function

$$R(s_t, a_t, s_{t+1}) : \mathcal{S} \times \mathcal{A} \times \mathcal{S} \rightarrow \mathbb{R}$$

gives the immediate reward for transitioning from state  $s_t \in \mathcal{S}$  to state  $s_{t+1} \in \mathcal{S}$  through action  $a_t \in \mathcal{A}$ . The observation distribution

$$O(o_t | s_t) : \mathcal{O} \times \mathcal{S} \rightarrow [0, 1]$$

gives the probability of getting observation  $o_t \in \mathcal{O}$  in state  $s_t \in \mathcal{S}$ . Finally,  $\gamma \in [0, 1]$  is a discount factor that scales the impact of future rewards.

When dealing with a POMDP in reinforcement learning, the agent cannot access the state  $s_t \in \mathcal{S}$  directly and must rely on the history  $\tau_t = (o_0, a_0, \dots, o_t) \in (\mathcal{O}, \mathcal{A})^t \times \mathcal{O} := \mathcal{T}_t$  since observations in a POMDP do not provide sufficient information as  $P(o_{t+1} | \tau_t, a_t) \neq P(o_{t+1} | o_t, a_t)$ .

Due to the unbounded growth of the history over time, a common approach is to encode the history into a fixed-size latent state using RNNs. This latent representation can then be used to learn a history-dependent policy with standard reinforcement learning algorithms.

## D Computation of the VAA

The variability among attractors (VAA) quantifies the level of multistability of an RNN  $f_\theta$  by measuring the number of different stable states reached by this model from a set of initial states  $\mathcal{H}$  under a constant input  $x$ . It returns the normalized number of different stable states, *i.e.*, a scalar between  $\frac{1}{|\mathcal{H}|}$ , when there is only one stable state, and 1, when all stable states are different. Mathematically, the VAA is defined as:

$$\text{VAA}(f_\theta, \mathcal{H}, x) = \frac{1}{|\mathcal{H}|} \sum_{i=1}^{|\mathcal{H}|} \frac{1}{\sum_{j=1}^{|\mathcal{H}|} \delta(\limsup_{n \rightarrow \infty} \|f_\theta^n(h_i, x) - f_\theta^n(h_j, x)\| = 0)},$$

where  $\delta(\cdot)$  is the Kronecker delta function and  $f^n$  is defined as:

$$f_\theta^n(h, x) = \begin{cases} f_\theta(f_\theta^{n-1}(h, x), x) & \text{if } n > 1, \\ f_\theta(h, x) & \text{if } n = 1. \end{cases}$$

However, the rigorous definition of the VAA implies computing limits to infinity, making it unusable in practice. Therefore, an approximation of the VAA is used in the experiments. This approximation introduces two parameters:  $M$ , the number of iterations of  $f$ , and  $\epsilon$ , the tolerance to consider two states as identical. Mathematically, it gives:

$$\text{VAA}(f_\theta, \mathcal{H}, x; M, \epsilon) = \frac{1}{|\mathcal{H}|} \sum_{i=1}^{|\mathcal{H}|} \frac{1}{\sum_{j=1}^{|\mathcal{H}|} \delta(\|f_\theta^M(h_i, x) - f_\theta^M(h_j, x)\| \leq \epsilon)}.$$

When computing VAA to a specific task, the set of initial states  $\mathcal{H}$  and the constant input  $x$  have to be defined. Two tasks are considered in this work, the classic T-maze and its variant, the Lookup-TreeMaze. Therefore  $\mathcal{H}$  and  $x$  must be defined for both. For the classic T-maze, we simply used the hidden states obtained at the first timestep after giving the position of the reward to the agent. As only two positions are allowed,  $|\mathcal{H}| = 2$ . For the LookupTreeMaze, we considered the hidden states obtained by feeding all possible lookup tables to the agent. For a lookup table of size  $n$ ,  $|\mathcal{H}| = 2^n - 2$  (as the lookup table where rewards are all up or all down are never used). For both, the constant input  $x$  is simply the observation given to the agent while it has not reached the junction.

## E Training Procedure and Hyperparameters

Given that the environments used in this work are partially observable Markov decision processes, the optimal policies and value functions are dependent on the sequence of all observations and actions (*i.e.*, the history). We use the proximal policy optimization (PPO) [32] algorithm, an advantage actor-critic [44] method, to approximate the optimal policy and the value function. The policy and the value function ( $\pi$  and VF respectively) are implemented with RNNs. Nothing is shared between the policy and the value function, so the history is encoded separately by both RNNs.

The policy neural network outputs a probability distribution over the action space from which the next action is sampled to encourage exploration at the beginning of the training and exploitation at the end as the distribution entropy decreases.

All models were trained using a modified version of the LSTM PPO implementation from CleanRL [45].

The following network was considered for the T-maze experiments shown in Figure 3 with the exception of the deep minGRU:

$$\text{RNN}_5 \rightarrow \text{ReLU}_{20} \rightarrow \text{ReLU}_{10} \rightarrow \text{FC}_{out},$$

where  $\text{FC}_N$  is a fully connected (or dense) layer of  $N$  neurons and  $\text{ReLU}_N$  is a fully connected layer of  $N$  neurons followed by a ReLU (rectified linear unit activation function).  $\text{RNN}_5$  is a recurrent layer of 5 neurons and is either GRU, BRC, or nBRC depending of the model. This architecture was used for the policy and the value function estimators. The size of the output is denoted *out* and its value is 4 for the policy and 1 for the value function.

For the deep minGRU, the following architecture was used:

$$\text{ReLU}_{128} \rightarrow \text{minGRU}_{128} \times 4 \rightarrow \text{Sum} \rightarrow \text{ReLU}_{64} \rightarrow \text{ReLU}_{16} \rightarrow \text{FC}_{out},$$

where  $\text{minGRU}_{128} \times 4$  denotes 4 minGRUs of 128 neurons in sequence, and Sum represents a skip connection as a sum between the output of  $\text{ReLU}_{128}$  and the output of the last  $\text{minGRU}_{128}$  followed by a ReLU.

In the LookupTreeMaze experiments shown in Figure 4, the following architecture was used:

$$\text{ReLU}_{128} \rightarrow \text{RNN}_{128} \rightarrow \text{Sum} \rightarrow \text{ReLU}_{64} \rightarrow \text{ReLU}_{16} \rightarrow \text{FC}_{out},$$

where all layers are followed by a Dropout layer with probability  $p = 0.1$  except for the last layer. In the case of the hybrid BMRU+minGRU architecture, the RNN layer is a concatenation of the output of a  $\text{BMRU}_{64}$  and a  $\text{minGRU}_{64}$ , both taking the same input.

Five different recurrent cells were considered: GRU, BRC, nBRC, minGRU, and BMRU. For each of these, 30 models were initialized with different seeds (from 1 to 30) and trained, for a total of 150 models for the T-maze experiment and 180 models for the LookupTreeMaze experiment.

The hyperparameters used for each experiment is shown in Table 1.

Table 1: Hyperparameters used during training for the two benchmarks.

Hyperparameter	Benchmark 1 (T-maze)	Benchmark 2 (LookupTreeMaze)
$\pi$ epochs	20	10
VF epochs	10	10
$\pi$ optimizer	Adam ( $lr = 0.005$ )	Adam ( $lr = 0.005$ )
VF optimizer	Adam ( $lr = 0.001$ )	Adam ( $lr = 0.001$ )
LR scheduler	Cosine annealing ( $T_{max} = 250$ )	Cosine annealing ( $T_{max} = 250$ )
Grad. clip norm	1	1
PPO $\epsilon_{clip}$	0.2	0.2
VF coeff. $c_1$	1	1
Entropy coeff. $c_2$	0.01	0.01
GAE ( $\lambda$ )	0.98	0.98
Discount ( $\gamma$ )	0.998	0.998
Minibatch ( $N \times \text{size}$ )	$2 \times 25$	$8 \times 256$
$\text{KL}_{max}$ early stop	0.2	0.2
Sample steps	1400	250
Total iterations	250	250

**Compute resources** All training experiments were performed on an academic HPC cluster, using a single NVIDIA Tesla A100 GPU (40 GB VRAM) per run on a node with AMD EPYC Milan CPUs and up to 512 GB of system RAM. The total compute footprint of the project, including preliminary experiments not reported in this paper, remains modest by modern deep learning standards.

## F T-maze Environment

We base our formal definition of the T-maze on the work of Lambrechts et al. [18]. The T-maze environment is a POMDP  $(\mathcal{S}, \mathcal{A}, \mathcal{O}, p_0, T, R, O, \gamma)$  parameterized by the maze length  $L \in \mathbb{Z}^+$ .

**State space** The discrete state space  $\mathcal{S}$  is composed of the position of the agent  $\mathcal{P}$  and the position of the goal  $\mathcal{G}$ , with

$$\begin{cases} \mathcal{S} = \mathcal{P} \times \mathcal{G} \\ \mathcal{P} = \{(0, 0), \dots, (L - 1, 0)\} \cup \{(L - 1, -1), (L - 1, 1)\} \\ \mathcal{G} = \{-1, 1\}, \end{cases}$$

where the -1 and 1 goal positions represent up and down respectively. Additionally, there are four terminal states given by the set  $\mathcal{F} = \{s_t = (p_t, g_t) \in \mathcal{S} \mid p_t \in \{(L - 1, -1), (L - 1, 1)\}, g_t \in \mathcal{G}\}$ .

**Action space** The discrete action space is composed of the four possible directions in which the agent can move and is defined as  $\mathcal{A} = [0, 3]$ , where each value correspond to the right, top, left, and down directions respectively.

**Observation space** The discrete observation space is composed of the initial observation of the goal at the first timestep, 0 otherwise, and a flag indicating whether the agent has reached the far right of the maze (1) or not (0). Formally, we have

$$\mathcal{O} = \{(g_t, f_t) \mid g_{t=0} \in \mathcal{G}, g_{t>0} = 0, f_t \in \{1, 0\}\}.$$

**Initial state distribution** The two possible initial states are  $s_0^{up} = ((0, 0), -1)$  and  $s_0^{down} = ((0, 0), 1)$ . The initial state distribution  $p_0 : \mathcal{S} \rightarrow [0, 1]$  is given by

$$p_0(s_0) = \begin{cases} 0.5 & \text{if } s_0 = s_0^{up}, \\ 0.5 & \text{if } s_0 = s_0^{down}, \\ 0 & \text{otherwise.} \end{cases}$$

**Transition distribution** The transition distribution function  $T : \mathcal{S} \times \mathcal{A} \times \mathcal{S} \rightarrow [0, 1]$  is given by

$$T(s_{t+1} \mid s_t, a_t) = \delta_{f(s_t, a_t)}(s_{t+1}),$$

where  $s_{t+1} \in \mathcal{S}$ ,  $s_t \in \mathcal{S}$  and  $a_t \in \mathcal{A}$ , and  $f$  is given by

$$f(s_t, a_t) = \begin{cases} s_{t+1} = (p_t + (1, 0), g_t) & \text{if } s_t \notin \mathcal{F}, p_t + (1, 0) \in \mathcal{P}, a_t = 0, \\ s_{t+1} = (p_t - (1, 0), g_t) & \text{if } s_t \notin \mathcal{F}, p_t - (1, 0) \in \mathcal{P}, a_t = 2, \\ s_{t+1} = (p_t + (0, 1), g_t) & \text{if } s_t \notin \mathcal{F}, p_t + (0, 1) \in \mathcal{P}, a_t = 3, \\ s_{t+1} = (p_t - (0, 1), g_t) & \text{if } s_t \notin \mathcal{F}, p_t - (0, 1) \in \mathcal{P}, a_t = 1, \\ s_{t+1} = (p_t, g_t) & \text{otherwise,} \end{cases}$$

where  $s_t = (p_t, g_t) \in \mathcal{S}$  and  $a_t \in \mathcal{A}$ .

**Reward function** The reward function  $R : \mathcal{S} \times \mathcal{A} \times \mathcal{S} \rightarrow \mathbb{R}$  is given by

$$R(s_t, a_t, s_{t+1}) = \begin{cases} 4 & \text{if } s_t \notin \mathcal{F}, s_{t+1} \in \mathcal{F}, p_{t+1} = (L - 1, g_0), \\ -0.1 & \text{if } s_t \notin \mathcal{F}, s_{t+1} \in \mathcal{F}, p_{t+1} = (L - 1, r), r \in \mathcal{G}, r \neq g_0 \\ 0 & \text{otherwise,} \end{cases}$$

where  $s_t = (p_t, g_t) \in \mathcal{S}$ ,  $a_t \in \mathcal{A}$ ,  $s_{t+1} = (p_{t+1}, g_{t+1}) \in \mathcal{S}$ .

**Observation distribution** The observations are deterministic. The observation distribution  $O : \mathcal{O} \times \mathcal{S} \rightarrow [0, 1]$  is given by

$$O(o_t \mid s_t) = \begin{cases} 1 & \text{if } o_t = (g_t, \delta(p_t = L - 1)), \\ 1 & \text{if } o_t = (0, \delta(p_t = L - 1)), \\ 0 & \text{otherwise,} \end{cases}$$

where  $o_t \in \mathcal{O}$  and  $s_t = (p_t, g_t) \in \mathcal{S}$ .

## G LookupTreeMaze Environment

The LookupTreeMaze environment is a POMDP  $(\mathcal{S}, \mathcal{A}, \mathcal{O}, p_0, T, R, O, \gamma)$  parameterized by the range of the number of T-mazes  $N := [N_{low}, N_{high}]$  with  $0 < N_{low} \leq N_{high}$ , the range of the maze lengths  $L := [L_{low}, L_{high}]$  with  $0 < L_{low} \leq L_{high}$ , and the size of the lookup table  $\tau \in \mathbb{Z}^{>1}$ .

**State space** The discrete state space  $\mathcal{S}$  is composed of the horizontal position of the agent in the current T-maze  $\mathcal{P}$ , the number of T-mazes in the current LookupTreeMaze  $\mathcal{B}$ , the index of the T-maze in which it is located  $\mathcal{K}$ , the position of the goal for the current T-maze  $\mathcal{G}$ , the length of the current T-maze  $\mathcal{L}$ , the lookup table  $\mathcal{D}$ , and a flag showing whether this is the first time the agent enters a new T-maze  $\mathcal{H}$ , with

$$\left\{ \begin{array}{l} \mathcal{S} = \mathcal{P} \times \mathbf{B} \times \mathcal{K} \times \mathcal{G} \times \mathcal{L} \times \mathcal{D} \times \mathcal{H} \\ \mathcal{P} = \{0, \dots, L_{high} - 1\} \\ \mathcal{B} = \{N_{low}, N_{high}\} \\ \mathcal{K} = \{0, \dots, N_{high}\} \\ \mathcal{G} = \{-1, 1\} \\ \mathcal{L} = \{L_{low}, \dots, L_{high}\} \\ \mathcal{D} = \mathcal{G}^\tau \setminus \{(g, \dots, g) \mid g \in \mathcal{G}\} \\ \mathcal{H} = \{1, 0\} \end{array} \right.$$

where the -1 and 1 goal positions represent up and down respectively. Additionally, the terminal states are given by the set

$$\mathcal{F} = \{s_t = (p_t, b_t, k_t, g_t, l_t, d_t, h_t) \in \mathcal{S} \mid p_t = 0, k_t = b_t, h_t = 0, \\ p_t \in \mathcal{P}, b_t \in \mathcal{B}, k_t \in \mathcal{K}, g_t \in \mathcal{G}, l_t \in \mathcal{L}, d_t \in \mathcal{D}\}.$$

**Action space** The discrete action space is composed of the four possible directions in which the agent can move and is defined as  $\mathcal{A} = [0, 3]$ , where each value correspond to the right, top, left, and down directions respectively.

**Observation space** The discrete observation space is composed of the lookup table at the first timestep, 0 otherwise, the index that references the direction of the next goal in the lookup table at the first timestep of each T-maze, otherwise 0, and a flag indicating whether the agent has reached the far right of the maze (1) or not (0). Formally, we have

$$\mathcal{O} = \{(d_t, i_t, f_t) \mid d_{t=0} \in \mathcal{D}, d_{t>0} \in \{0\}^\tau, i_t \in \{0, \dots, \tau - 1\}, d_{t, i_t} = g_t, h_t = 1, f_t \in \{1, 0\}\} \cup \\ \{(d_t, i_t, f_t) \mid d_{t=0} \in \mathcal{D}, d_{t>0} \in \{0\}^\tau, i_t = 0, h_t = 0, f_t \in \{1, 0\}\},$$

where  $g_t \in \mathcal{G}$ , and  $h_t \in \mathcal{H}$ .

**Initial state distribution** The number of T-mazes is uniformly sampled in the range  $N$ . Thus, the probability for a number of T-mazes  $n \in N$  is

$$p(n) = \frac{1}{N_{high} - N_{low} + 1}.$$

Similarly, the size of each T-maze is uniformly sampled in the range  $L$ . For each T-maze, the probability that its size is  $l \in L$  is

$$p(l) = \frac{1}{L_{high} - L_{low} + 1}.$$

For each T-maze, the goal is uniformly sampled and the probability of goal  $g \in \mathcal{G}$  is

$$p(g) = \frac{1}{2}.$$

Finally, the lookup table is uniformly sampled and, since there are  $2^\tau - 2$  possible tables, the probability of table  $d \in \mathcal{D}$  is

$$p(d) = \frac{1}{2^\tau - 2}.$$

**Transition distribution** The transition distribution function  $T : \mathcal{S} \times \mathcal{A} \times \mathcal{S} \rightarrow [0, 1]$  is given by

$$T(s_{t+1} \mid s_t, a_t) = \delta_{f(s_t, a_t)}(s_{t+1}),$$

where  $s_{t+1} \in \mathcal{S}$ ,  $s_t \in \mathcal{S}$  and  $a_t \in \mathcal{A}$ , and  $f$  is given by

$$f(s_t, a_t) = \begin{cases} s_{t+1} = (p_t + 1, b_t, k_t, g_t, l_t, d_t, 0) & \text{if } s_t \notin \mathcal{F}, p_t + 1 \in \mathcal{P}, a_t = 0, \\ s_{t+1} = (p_t - 1, b_t, k_t, g_t, l_t, d_t, 0) & \text{if } s_t \notin \mathcal{F}, p_t - 1 \in \mathcal{P}, a_t = 2, \\ s_{t+1} = (0, b_t, k_t + 1, \sim p_g(\cdot), \sim p_l(\cdot), d_t, 1) & \text{if } s_t \notin \mathcal{F}, p_t = l_t - 1, a_t \in \{1, 3\}, k_t + 1 < b_t, \\ s_{t+1} = (0, b_t, k_t + 1, g_t, l_t, d_t, 0) & \text{if } s_t \notin \mathcal{F}, p_t = l_t - 1, a_t \in \{1, 3\}, k_t + 1 = b_t, \\ s_{t+1} = (p_t, b_t, k_t, g_t, l_t, d_t, 0) & \text{otherwise,} \end{cases}$$

where  $s_t = (p_t, b_t, k_t, g_t, l_t, d_t, h_t) \in \mathcal{S}$ ,  $a_t \in \mathcal{A}$ , and  $p_g$  and  $p_l$  are the probability distribution defined previously for the goal and T-maze length respectively.

**Reward function** The reward function  $R : \mathcal{S} \times \mathcal{A} \times \mathcal{S} \rightarrow \mathbb{R}$  is given by

$$R(s_t, a_t, s_{t+1}) = \begin{cases} \frac{4}{b_t} & \text{if } s_t \notin \mathcal{F}, p_t = l_t - 1, a_t = 3, g_t = 1, \\ \frac{4}{b_t} & \text{if } s_t \notin \mathcal{F}, p_t = l_t - 1, a_t = 1, g_t = -1, \\ \frac{-0.1}{b_t} & \text{if } s_t \notin \mathcal{F}, p_t = l_t - 1, a_t = 3, g_t = -1, \\ \frac{-0.1}{b_t} & \text{if } s_t \notin \mathcal{F}, p_t = l_t - 1, a_t = 1, g_t = 1, \\ 0 & \text{otherwise,} \end{cases}$$

where  $s_t = (p_t, b_t, k_t, g_t, l_t, d_t, h_t) \in \mathcal{S}$ ,  $a_t \in \mathcal{A}$ ,  $s_{t+1} = (p_{t+1}, b_{t+1}, k_{t+1}, g_{t+1}, l_{t+1}, d_{t+1}, h_{t+1}) \in \mathcal{S}$ .

**Observation distribution** If we assume that 1 is present  $n$  times in the lookup table with  $0 < n < \tau$  (and consequently  $-1$  is present  $\tau - n$  times in the table), the probability for index  $i$  is

$$\begin{cases} p(i | g_t = 1) = \frac{1}{n} \\ p(i | g_t = -1) = \frac{1}{\tau - n}, \end{cases}$$

where  $g_t \in \mathcal{G}$ , and  $d_{t,i} = g_t$  with  $d_t \in \mathcal{D}$ . The rest of the observation is deterministic.

## H Equations for the different RNNs used in this work

The equations for the different models used in this paper are provided below. In each equation,  $W$  are learnable weight matrices,  $b$  and  $w$  are learnable parameter vectors,  $x_t$  in the input,  $h_t$  is the state, and  $r_t$ ,  $z_t$  and  $n_t$  are gate variables.  $H(\cdot)$  denotes the Heaviside step function, and  $S(\cdot)$  is the sign function.

### H.1 GRU [14]

$$\begin{aligned} r_t &= \sigma(W_{xr}x_t + W_{hr}h_{t-1} + b_r) \\ z_t &= \sigma(W_{xz}x_t + W_{hz}h_{t-1} + b_z) \\ n_t &= \tanh(W_{xn}x_t + r_t \odot W_{hn}h_{t-1} + b_n) \\ h_t &= z_t \odot h_{t-1} + (1 - z_t) \odot n_t \end{aligned}$$

### H.2 BRC [16]

$$\begin{aligned} r_t &= 1 + \tanh(W_r x_t + w_r \odot h_{t-1} + b_r) \\ z_t &= \sigma(W_z x_t + w_z \odot h_{t-1} + b_z) \\ n_t &= \tanh(W_n x_t + r_t \odot h_{t-1} + b_n) \\ h_t &= z_t \odot h_{t-1} + (1 - z_t) \odot n_t \end{aligned}$$

### H.3 nBRC [16]

$$\begin{aligned} r_t &= 1 + \tanh(W_{xr}x_t + W_{hr}h_{t-1} + b_r) \\ z_t &= \sigma(W_{xz}x_t + W_{hz}h_{t-1} + b_z) \\ n_t &= \tanh(W_n x_t + r_t \odot h_{t-1} + b_n) \\ h_t &= z_t \odot h_{t-1} + (1 - z_t) \odot n_t \end{aligned}$$

### H.4 minGRU [10]

$$\begin{aligned} z_t &= \sigma(W_z x_t + b_z) \\ n_t &= W_n x_t + b_n \\ h_t &= z_t \odot h_{t-1} + (1 - z_t) \odot n_t \end{aligned}$$

## H.5 BMRU [12]

$$\begin{aligned}
 n_t &= W_n x_t + b_n \\
 \beta_t &= |W_\beta x_t + b_\beta| \\
 z_t &= \mathbf{H}(|n_t| - \beta_t) \\
 h_t &= z_t \odot \mathbf{S}(n_t) \odot \alpha + (1 - z_t) \odot h_{t-1}
 \end{aligned}$$

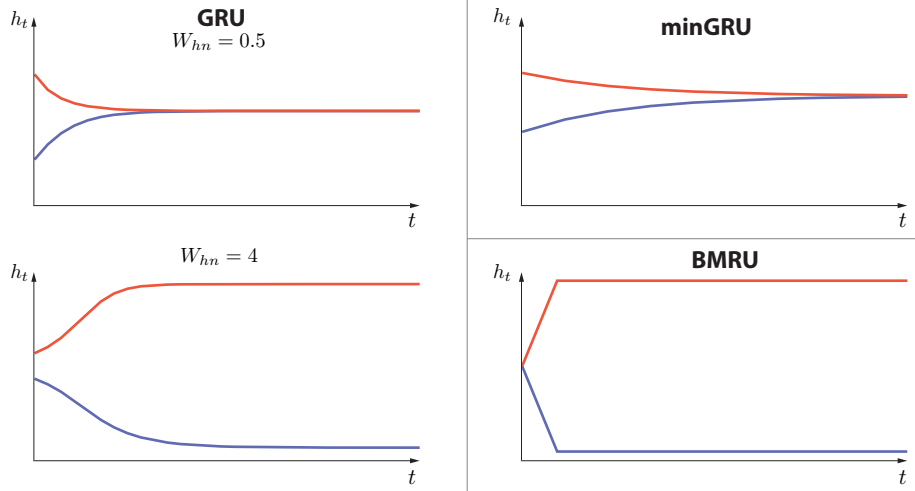


Figure 5: Left, time evolution of the internal state of a single GRU for two different initial conditions (red and blue curves) and two different values of  $W_{hn}$ . The top graph shows a monostable behavior: both initial conditions reach the same equilibrium. The bottom graph shows a bistable behavior: each initial condition reaches a different equilibrium. Right, time evolution of the internal state of a single minGRU (top) and BMRU (bottom) for two different initial conditions (red and blue curves). minGRU exhibits monostable behavior with transient dynamics, whereas BMRU exhibit bistable behavior with a one step convergence.

## I Learning curves and RNN dynamics

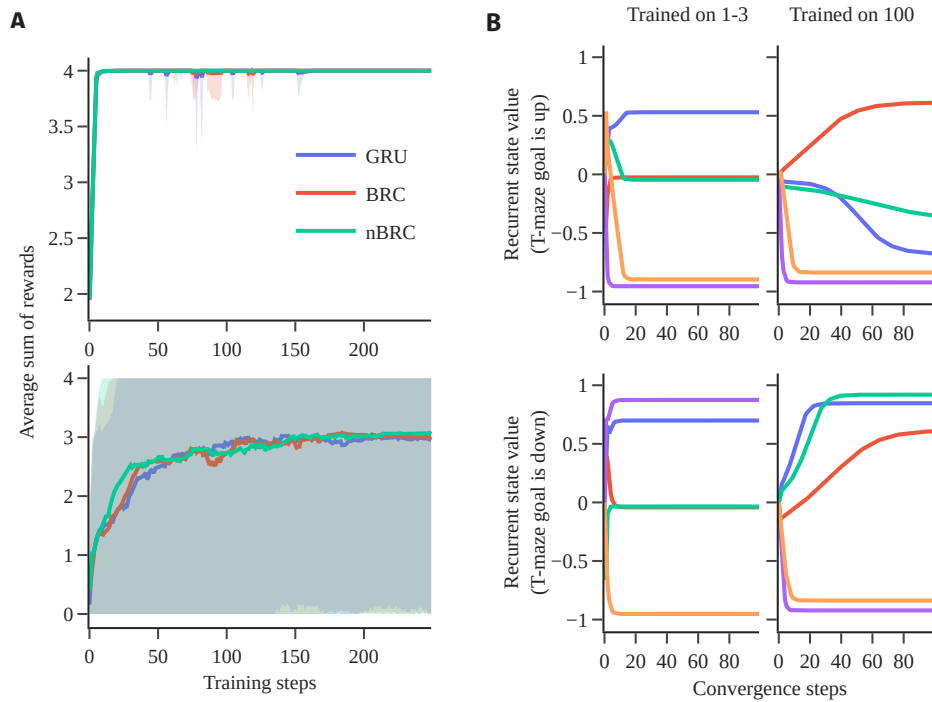


Figure 6: **A.** Evolution of the average sum of rewards (with  $2\sigma$ ) obtained by the agents during their training on T-mazes of lengths 1-3 (top), and of length 100 (bottom). **B.** Time evolution of the internal states of two bistable models, one trained on small T-mazes (left), the other trained on long T-mazes (right), for the two possible cases on a T-maze of length 100. The figure shows that models trained on long T-mazes have slower transient dynamics before reaching equilibrium.